

# Development of a Wide-Band Short Backfire Antenna Excited by an Unbalance-Fed H-Shaped Slot

RongLin Li, *Senior Member, IEEE*, Dane Thompson, *Student Member, IEEE*,  
Manos M. Tentzeris, *Senior Member, IEEE*, Joy Laskar, *Senior Member, IEEE*, and  
John Papapolymou, *Senior Member, IEEE*

**Abstract**—The short backfire antenna (SBA) has been widely used for mobile satellite communications, tracking, telemetry, and wireless local-area network applications due to its compact structure and excellent radiation characteristics. The most common excitation topology for the SBA is a balance-fed wire dipole, which has the disadvantage of a narrow frequency bandwidth for the input impedance. In this paper, an H-shaped slot is employed to excite the SBA for the first time. The H-shaped slot is unbalance-fed from a coaxial line. It is demonstrated that the H-shaped slot-excited SBA can achieve a bandwidth for input impedance of more than 20% ( $VSWR < 2$ ) while maintaining good radiation performance. The antenna structure is described and the simulation and experimental results are presented. The operating principle is investigated to explain why the slot-excited SBA can result in good impedance and radiation characteristics. A parametric study is conducted for the use of practical engineering design.

**Index Terms**—Short backfire antenna, slot-fed antenna, wide-band antenna.

## I. INTRODUCTION

THE short backfire antenna (SBA) was first developed by Ehrenspeck in the 1960s [1], [2]. This type of antenna usually consists of a half-wavelength ( $\lambda_0/2$ ,  $\lambda_0$  is the free-space wavelength at operating frequency) dipole exciting antenna, a pair of planar reflectors, and a rim. The exciting dipole is centered between the two reflectors which have a diameter of about  $2.0\lambda_0$  and  $0.4\lambda_0$ , respectively, and are separated by a spacing of  $0.5\lambda_0$ . The rim with a height of about  $0.25\lambda_0$  surrounds the larger reflector. The SBA can achieve a gain on the order of 13–15 dBi, with sidelobes of at least  $-20$  dB and a backlobe level lower than  $-30$  dB [3]. In addition to its excellent radiation characteristics, the SBA is very attractive to mobile/maritime satellite communications, tracking, telemetry, and wireless local-area network (WLAN) applications [4], [5] due to its compact structure ( $0.5\lambda_0$  in height) and simple feed configuration (a single dipole rather than an array).

Since it is essentially a leaky cavity structure for which the excitation is provided by the primary dipole source, the dipole-excited SBA has a narrow frequency bandwidth for its input impedance. The natural impedance match bandwidth is only 3–5% for the voltage standing wave ratio (VSWR) under 1.5

[6], [7]. This situation becomes even worse as the height of the rim increases for suppressing the sidelobe level [8]. Our investigation shows that the bandwidth of a dipole-excited SBA is less than 1% for  $VSWR < 2$  when the rim height rises to  $0.5\lambda_0$  if without a matching circuit. In addition, a balun is necessary for the balance-fed dipole “exciter.”

An alternative excitation configuration is the waveguide feed system, such as coaxial or rectangular waveguide feed [9], [10]. Unfortunately, the waveguide-excited SBA requires a bulky feeding structure. Another candidate for the SBA excitation may be the patch antenna. But there are two problems that need to be resolved before this approach can be used to excite the SBA. First, if the patch antenna is located too low, the bandwidth for impedance may be very narrow and also it is more difficult to excite the leaky waves required for the backfire radiation. On the other hand, if increasing the height of the exciting patch, the feed probe needs to be longer, which results in an increased inductive component in the input impedance due to the parasitic inductance from the feed probe, thus causing a matching difficulty. Furthermore, a longer feed probe will produce a higher cross-polarized component, degrading the excellent radiation performance for the SBA.

Recently, it has been demonstrated that a center-fed slotted patch antenna can considerably enhance the impedance and radiation performances even though the patch is suspended about  $0.1\lambda_0$  high over a ground plane [11]. Essentially the enhanced performances are mainly attributed to the unbalance-fed slot that is formed at the center of the patch antenna. In this paper, we propose to make use of the configuration of unbalance-fed slot on a suspended patch for the SBA excitation for the first time. Instead of using a rectangular slot as in [11], we employ an H-shaped slot since it has more degrees of design freedom for antenna performance optimization [12]. Also the slotted patch can be positioned much higher than  $0.1\lambda_0$  (about  $0.32\lambda_0$ ) required for the impedance match of the slot-excited SBA. As will be discussed later, the unbalanced feed acts as a two-wire transmission line, hence avoiding the difficulties for a longer feed probe, such as the increased parasitic inductance and the higher cross-polarized component. The antenna structure for the proposed SBA is described first, followed by simulation and experimental results. The mechanism of operation for good impedance and radiation performances is investigated comprehensively. It will be clarified why the unbalance-fed slot can excite the backfire radiating mode for the SBA and how the exciting slot can be matched to a  $50\text{-}\Omega$  feed. Finally, a parametric study is presented for the potential need in practical engineering design.

Manuscript received January 21, 2004; revised June 13, 2004. This work was supported in part by the Georgia Electronic Design Center, in part by the National Science Foundation (NSF) under CAREER Award ECS-9984761 and Grant ECS-0313951, and in part by the NSF Packaging Research Center.

The authors are with the Georgia Electronic Design Center, School of Electrical and Computer Engineering, Georgia Institute of Technology, Atlanta, GA 30332-0250 USA (e-mail: rlli@ece.gatech.edu).

Digital Object Identifier 10.1109/TAP.2004.841291

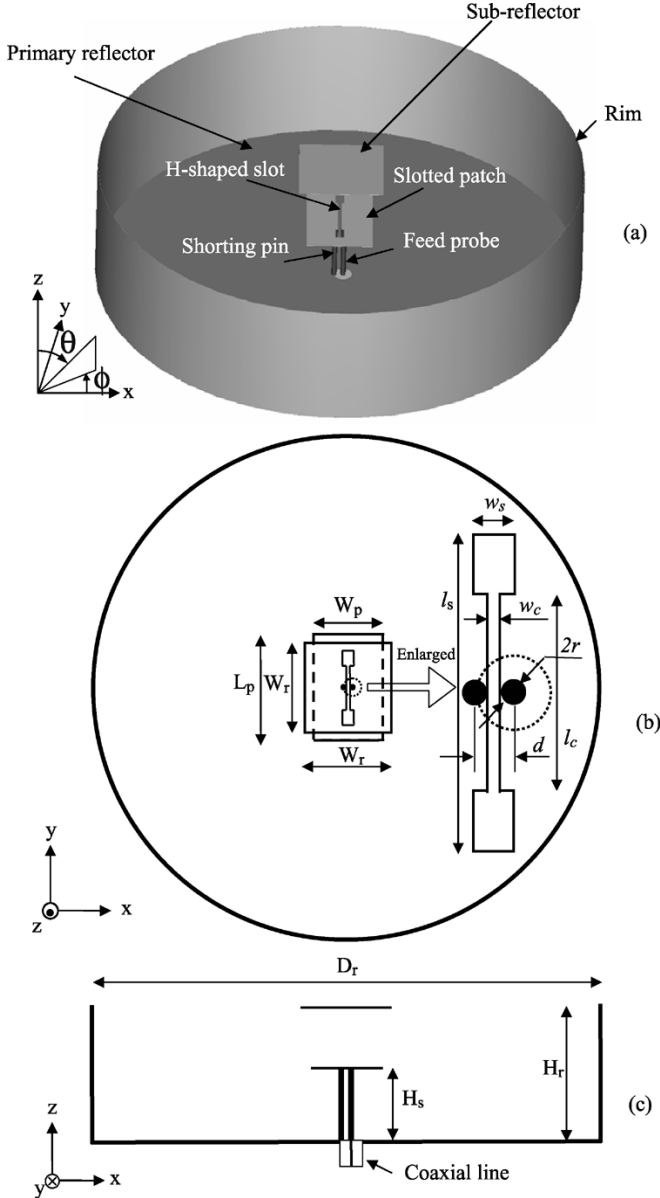


Fig. 1. SBA excited by an unbalance-fed H-shaped slot: (a) 3-D configuration, (b) top view, and (c) front view.

## II. DESCRIPTION OF ANTENNA

The three-dimensional (3-D) configuration of the slot-excited SBA is depicted in Fig. 1(a). Similar to the conventional SBA, the proposed SBA contains a pair of reflectors (i.e., a circular primary reflector and a square subreflector) and a circular rim. For accurate numerical modeling, we chose a square instead of a circular plate for the subreflector. This choice does not lead to a significant effect on the antenna performance. Instead of being excited by a dipole, the proposed SBA is excited by an H-shaped slot which has been cut on a rectangular patch. The H-shaped slot is center-fed at one side of the slot by a cylindrical wire probe that has been extended from the inner conductor of a coaxial line. The other side of the slot is shorted to the primary reflector through a straight pin which has the same size as the feed probe. All dimensions of the SBA are illustrated in Fig. 1(b) (top view) and (c) (front view). Like the dipole-excited SBA, the dimensions of two reflectors and the rim can be

TABLE I  
OPTIMIZED GEOMETRIC PARAMETERS FOR THE SLOT-EXCITED SBA ( $\lambda_0 =$   
THE FREE-SPACE WAVELENGTH AT THE DESIGN FREQUENCY)

$D_r$	$2.20\lambda_0$	$l_s$	$0.32\lambda_0$
$H_r$	$0.58\lambda_0$	$l_c$	$0.20\lambda_0$
$H_s$	$0.32\lambda_0$	$w_s$	$0.04\lambda_0$
$W_r$	$0.38\lambda_0$	$w_c$	$0.016\lambda_0$
$W_p$	$0.30\lambda_0$	$r$	$0.012\lambda_0$
$L_p$	$0.46\lambda_0$	$d$	$0.040\lambda_0$

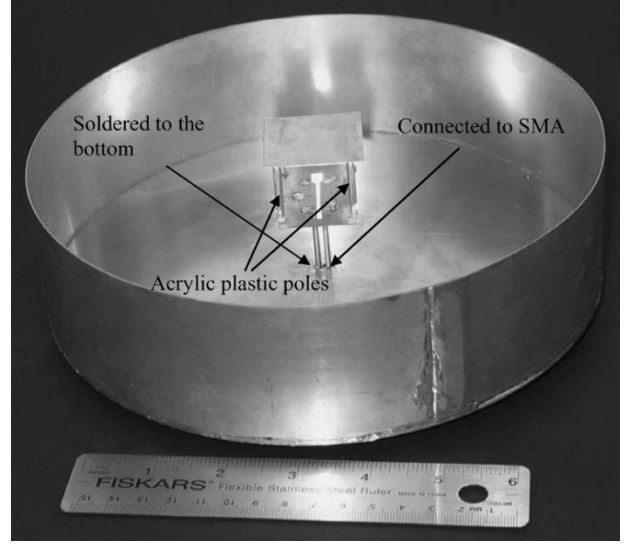


Fig. 2. Photograph of a prototype of the slot-excited SBA.

adjusted for a desirable radiation performance, such as a higher gain or/and a lower sidelobe level [13], [14]. Here choosing the rim and the subreflector to have the same height ( $H_r$ ) is based on two considerations: a) to minimize the sidelobe level and b) to make the whole structure of the SBA look like a “can,” which may be helpful in high-volume production since the subreflector can serve as part of the cover (or radome) of the “can” (or the SBA). The dimensions of the H-shaped slot, the feed probe, and the shorting pin are optimized for a good impedance performance, i.e., a wide bandwidth for input impedance. Following a large number of numerical simulations, we got the optimized geometric parameters shown in Table I. The overall dimensions of optimized SBA are  $0.58\lambda_0$  in height and  $2.2\lambda_0$  in diameter, which are slightly larger than those (typically  $0.5\lambda_0$  in height and  $2\lambda_0$  in diameter) for a dipole-excited SBA. The reason for the larger dimensions will be explained in the next sections.

To demonstrate the performance of the new SBA experimentally, we fabricated a prototype of the antenna designed to operate in the  $S$  band (the design frequency = 3 GHz). Fig. 2 shows a photograph of the prototype. The reflectors, rim, and slotted patch were built using alloy 260 brass plates. The metal thickness of the slotted patch and the subreflector is 0.25 mm. The shorting pin and feed probe are made of a cylindrical alloy wire whose diameter is 2.4 mm. A semiminaturized type-A (SMA) connector is connected to the feed probe from the backside of the primary reflector. The slotted patch is supported by making use of the shorting pin and the feed probe while the subreflector is supported by four acrylic plastic poles.

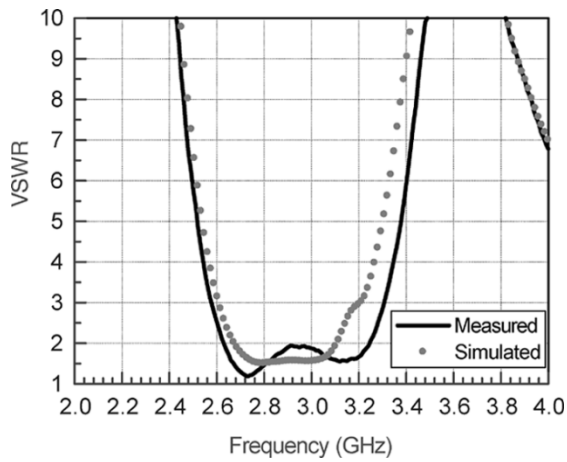


Fig. 3. Measured and simulated VSWR for the slot-excited SBA.

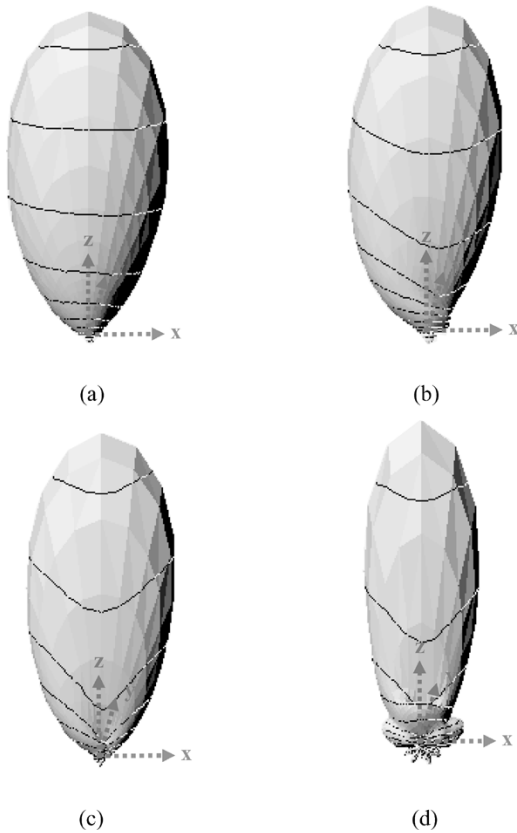


Fig. 4. Simulated 3-D radiation patterns of the slot-excited SBA (normalized on linear scale): (a) at 2.6 GHz, (b) at 2.8 GHz, (c) at 3.0 GHz, and (d) at 3.2 GHz.

### III. SIMULATION AND EXPERIMENTAL RESULTS

The numerical simulation was accomplished by using the transmission line matrix (TLM) technique-based software Microstripes 6.0. Fig. 3 shows the simulated and measured results for VSWR of the slot-excited SBA. We can see good agreement between the simulated and measured results. The measured bandwidth for  $VSWR < 2$  is found to be about 20%. The 3-D radiation patterns calculated at 2.6, 2.8, 3.0, and 3.2 GHz are shown in Fig. 4, demonstrating very low backlobe level and no obvious sidelobes for the frequencies below 3.0 GHz. The beamwidth decreases as the frequency increases because the

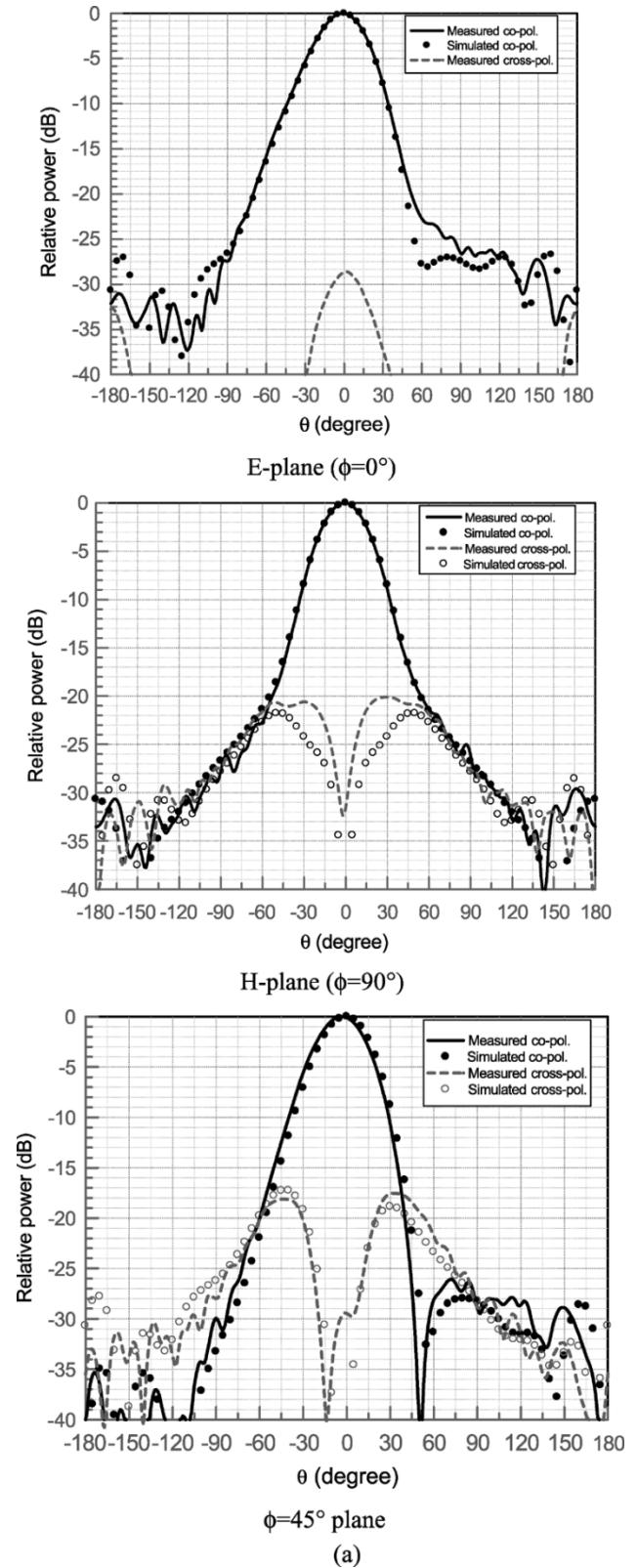
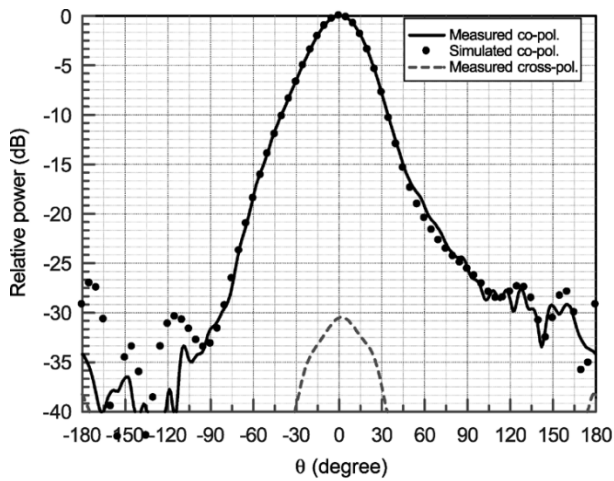
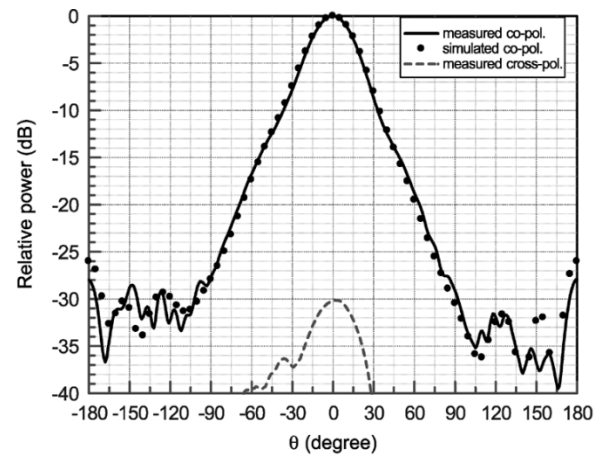


Fig. 5. Comparison of measured and simulated radiation patterns. (a) At 2.7 GHz.

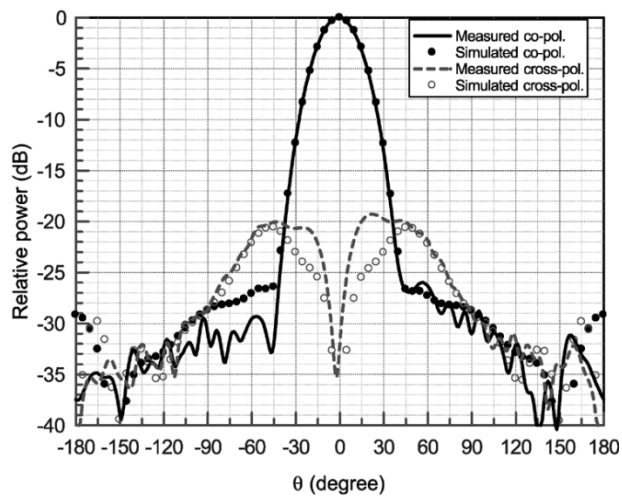
electrical size of the antenna aperture increases with frequency. The comparison between the measured E-plane, H-plane, and  $\phi = 45^\circ$  plane patterns and the simulations is shown in Fig. 5 at frequencies 2.7, 2.9, and 3.1 GHz. The agreement between the measured and simulated results is good over the main beam



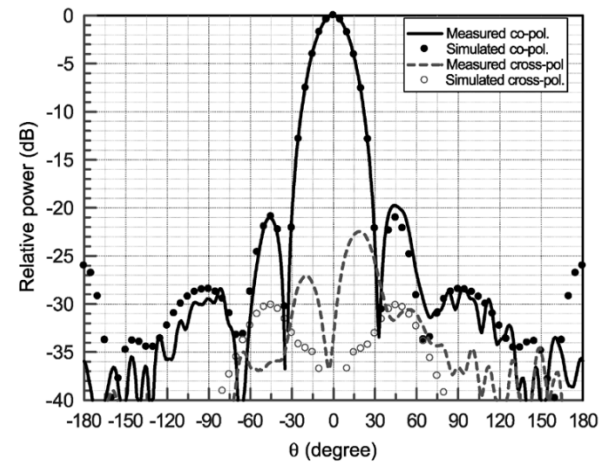
E-plane ( $\phi=0^\circ$ )



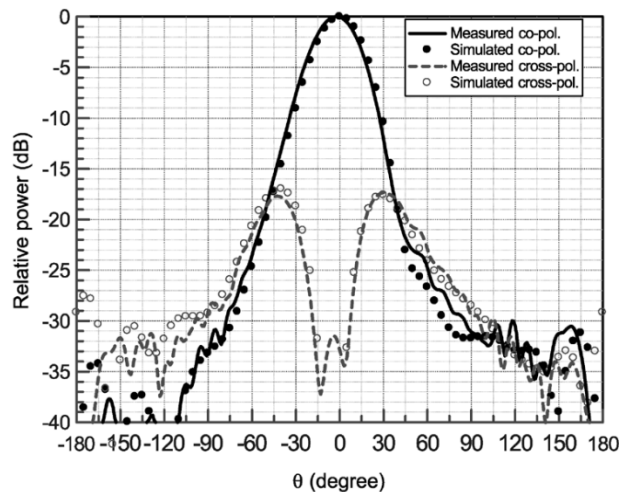
E-plane ( $\phi=0^\circ$ )



H-plane ( $\phi=90^\circ$ )

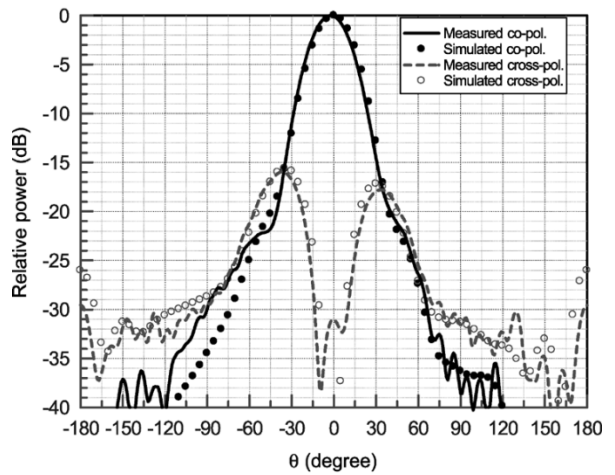


H-plane ( $\phi=90^\circ$ )



$\phi=45^\circ$  plane

(b)



$\phi=45^\circ$  plane

(c)

Fig. 5. (Continued.) Comparison of measured and simulated radiation patterns. (b) At 2.9 GHz.

Fig. 5. (Continued.) Comparison of measured and simulated radiation patterns. (c) At 3.1 GHz.

region. The sidelobe level is lower than  $-20$  dB while the peak backlobe is smaller than  $-25$  dB, comparable to those results for a dipole-excited SBA [8]. Similar to the dipole-excited SBA, the slot-excited SBA has a peak cross-polarized component in

the  $\phi = 45^\circ$  plane with a value of around  $-17$  dB, which is slightly higher than the  $-20$  dB for the dipole-excited SBA [14]. Note that the peak of the cross-polarization appears beyond the half-power main beam region. The cross-polarization level is

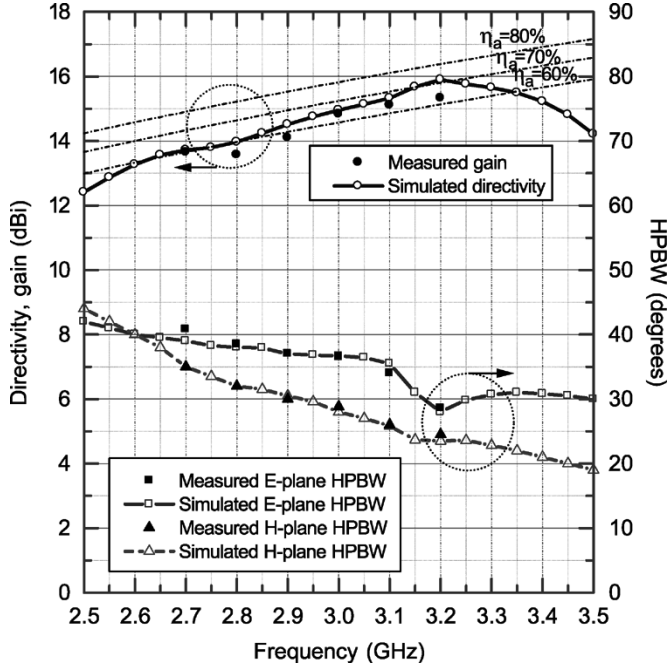


Fig. 6. Directivity, gain, and HPBW as a function of frequency.

lower than  $-20$  dB over the region  $-15^\circ < \theta < +15^\circ$ . The simulated directivity and measured power gain are plotted in Fig. 6 as a function of frequency. We can see that the power gain, varying between 13.5 and 15.5 dBi over 2.7–3.2 GHz, is only slightly lower than the directivity. This implies high radiation efficiency for the proposed SBA. In fact, our simulation reveals that the radiation efficiency of the SBA (a conductivity of  $1.6 \times 10^7$  S/m was used in the simulation for the whole antenna structure) is higher than 95% over the frequency range of 2.6–3.2 GHz. The simulated and measured results for the half-power beamwidth (HPBW) also agree well (see Fig. 6). In the frequency band 2.6–3.2 GHz, the HPBW in the E-plane is about  $0$ – $10^\circ$  wider than that in the H-plane. It is also noted that as frequency increases, the HPBW in the H-plane decreases (from  $40^\circ$  to  $20^\circ$ ) faster than the HPBW varies (from  $40^\circ$  to  $30^\circ$ ) in the E-plane due to the increase in the electrical length of the exciting slot whose longitudinal direction is parallel to the H-plane. It is the wider beamwidth in the E-plane that causes the directivity for the slot-excited SBA to be lower than that for a dipole-excited SBA. In turn, the aperture efficiency ( $\eta_a = 60$ – $70\%$ ; also see Fig. 6) of the new SBA is lower than that (about  $80\%$ ) of the dipole-excited SBA [8]. This explains why we need a slightly larger antenna aperture (i.e.,  $D_r = 2.2\lambda_0$ ) for a gain (about 15 dBi) that the dipole-excited SBA can achieve with an aperture diameter of  $2.0\lambda_0$ .

#### IV. OPERATING PRINCIPLE

##### A. Mode Analysis of the Unbalanced Feed

Similar to the analysis of folded dipole antennas [15], the unbalanced feed [Fig. 7(a)] of the SBA can be decomposed into two distinct driving modes: an even mode [Fig. 7(b)] and an odd mode [Fig. 7(c)]. Note that the voltage  $V$  in the odd mode comes from a combination of two series-connected voltage sources with the same polarity and amplitude ( $V/2$ ). The input current

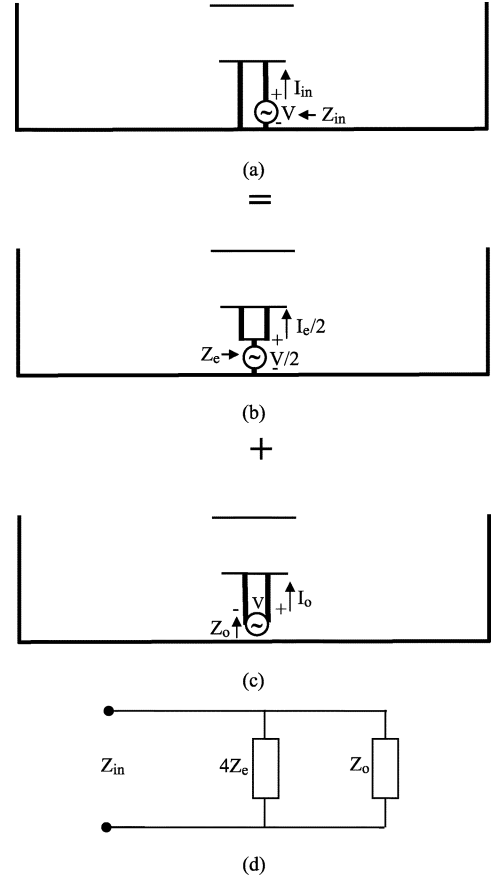


Fig. 7. Equivalent mode decomposition of the unbalance-fed SBA. (a) Unbalanced feed, (b) even mode, (c) odd mode, and (d) equivalent circuit for unbalanced input impedance  $Z_{in}$  for impedance.

$I_{in}$  excited on the feed probe by the unbalanced feed can be viewed as a superposition of effects excited by the even mode and the odd mode, that is

$$I_{in} = \frac{I_e}{2} + I_o = \frac{V}{4Z_e} + \frac{V}{Z_o} = \frac{V(Z_o + 4Z_e)}{4Z_e Z_o} \quad (1)$$

where the even-mode current  $I_e$  is equal to the even-mode voltage ( $V/2$ ) divided by the even-mode impedance  $Z_e$  [also see Fig. 7(b)] while the odd-mode current  $I_o$  is equal to the odd-mode voltage ( $V$ ) divided by the odd-mode impedance  $Z_o$  [also see Fig. 7(c)]. From (1), we can see that the unbalanced input impedance is equal to the parallel combination of the odd-mode impedance and the four times even-mode impedance

$$Z_{in} = \frac{V}{I_{in}} = \frac{4Z_e Z_o}{Z_o + 4Z_e}. \quad (2)$$

The equivalent circuit for the input impedance is drawn in Fig. 7(d).

To demonstrate the analysis, we simulated the even- and odd-mode feeds, respectively. The results for the even-mode and odd-mode impedances are shown in Fig. 8(a) and (b). The input impedance calculated by using (2) is compared in Fig. 8(c) to that obtained by direct simulation with an unbalance feed. Good agreement is observed. This validates the mode decomposition, thus implying that the radiation pattern of the unbalance-fed SBA can be viewed as a combination of the

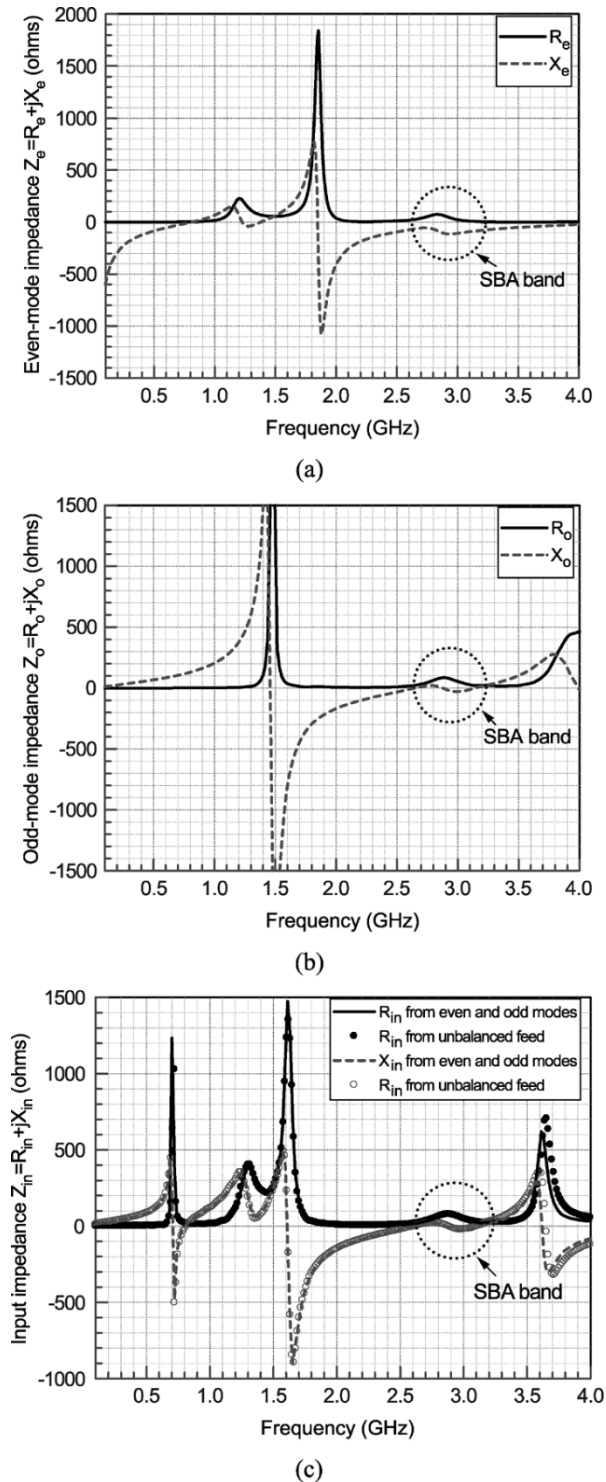


Fig. 8. Even- and odd-mode impedance and comparison of their combination with the simulated unbalance-mode impedance. (a) Even-mode impedance, (b) odd-mode impedance, and (c) comparison of input impedance between the results calculated by (2) and obtained by direct simulation with an unbalance feed.

even-mode and odd-mode excited radiation fields. Note that the even-mode excited SBA acts just like a vertical top-loaded monopole, which has no contribution to the radiation fields in the backfire direction (i.e., the  $z$ -direction). Instead, the even-mode excitation is the major contributor to the cross-polarized component. Therefore the even-mode current should be limited as low as possible over the frequency band (called

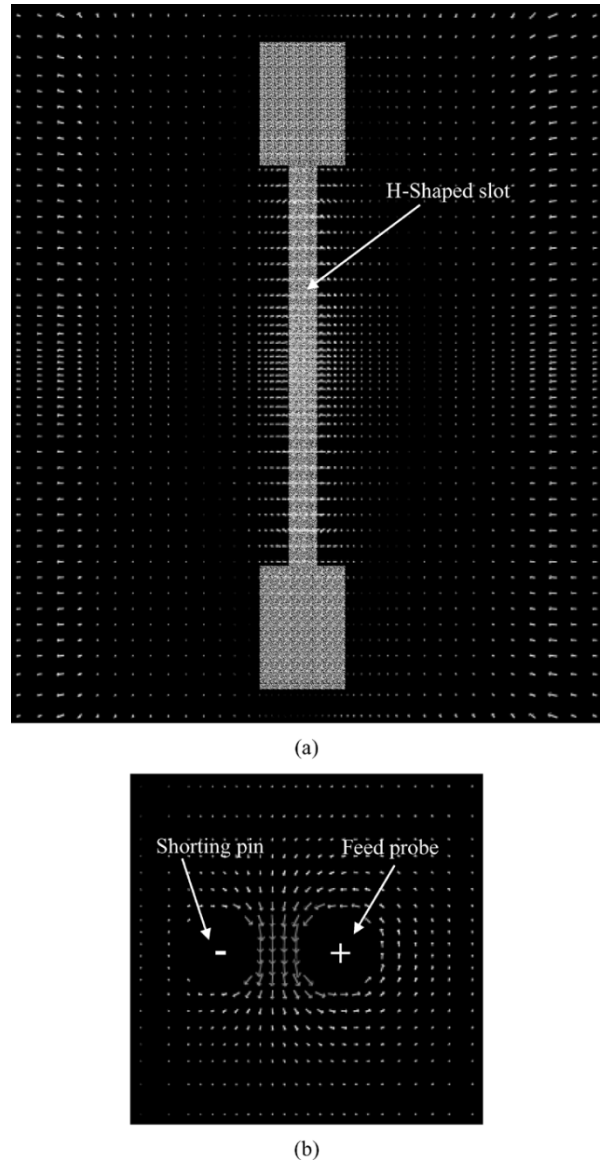


Fig. 9. Near-field distributions of the unbalance-fed H-shaped slot (at 3 GHz). (a) Electric-field distribution over the H-shaped slot and (b) magnetic-field distribution around the feed probe and shorting pin.

SBA band) for the backfire radiation. This can be achieved if the impedance related to the even mode is much higher than the odd-mode impedance. Interestingly, the even-mode impedance shown in Fig. 8(a) indeed has a quite strong (also relatively constant) reactive component (about  $100 \Omega$ ) in the SBA band (2.6–3.2 GHz). After being multiplied by a factor of four, the impedance related to the even mode is almost eight times greater than the odd-mode impedance (around  $50 \Omega$ ). As a result, the input impedance is mainly determined by the odd-mode impedance while the odd-mode current is the dominate excitation, which is definitely desirable for the backfire operation. To verify the odd-mode domination, the near-field distributions near the slot and the feed probe have been plotted in Fig. 9. Fig. 9(a) shows the electric-field distribution on the slot while Fig. 9(b) exhibits the magnetic-field around the feeding structure. Clearly, it does show an odd-mode field distribution: the electric field lines terminate on the two sides of the slot, whereas the magnetic field lines close on themselves

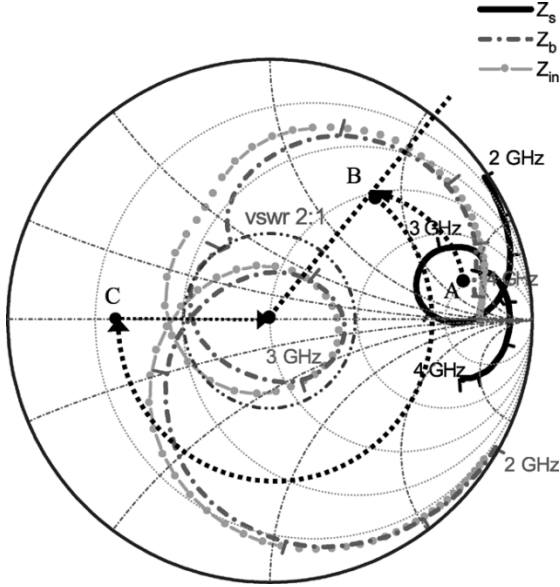


Fig. 10. Impedance matching of the slot-excited SBA.

around the feed probe and the shorting pin. Of course, the far-field pattern (i.e., the backfire pattern) described before also confirms the odd-mode operation over the SBA band.

### B. Mechanism for Impedance Matching

It is well known that a slot antenna usually has input impedance much larger than  $50 \Omega$ . If we feed the slot-excited SBA with a balanced mode (e.g., by a two-wire transmission line), a transformer (or a balun) is needed between the transmission line and a  $50\text{-}\Omega$  source. Interestingly, as demonstrated before, the unbalanced feed system formed by a feed probe and a shorting pin can automatically match to a  $50\text{-}\Omega$  coaxial line. The reason for the automatic matching is that the feed probe and shorting pin form a two-wire “transmission line,” which can convert a large impedance into a  $50\text{-}\Omega$  resistance if properly adjusting the length of the “transmission line.”

To demonstrate this argument, we first calculate the input impedance (called  $Z_s$ ) as a voltage source is directly connected across the center of the slot. The result is plotted in a Smith chart, as shown in Fig. 10. The impedance loci form a loop on the right side of the Smith chart, which implies a wide-band feature (mainly due to the coupling between the slotted patch and the subreflector) but with an impedance much larger than  $50 \Omega$ . We can transform the impedance  $Z_s$  into the input impedance (called  $Z_b$ ) observed at the bottom of the SBA by applying the transmission-line formula

$$Z_b = Z_c \frac{Z_s + jZ_c \tan \beta H_s}{Z_c + jZ_s \tan \beta H_s} \quad (3)$$

where  $\beta = 2\pi/\lambda_0$ ,  $H_s$  is the height of the slotted patch, and  $Z_c$  is the characteristic impedance of the two-wire (the feed probe and the shorting pin) “transmission line.” The two-wire characteristic impedance can be calculated by [16]

$$Z_c = 120 \ln \left[ \frac{d}{2r} + \sqrt{\left(\frac{d}{2r}\right)^2 - 1} \right] \quad (4)$$

where  $r$  is the wire radius for the feed probe and short pin and  $d$  is the center-to-center distance between the feed probe and the short pin. For the optimized structure, substituting  $d = 0.040\lambda_0$  and  $r = 0.012\lambda_0$  into (4), we obtain  $Z_c = 120 \ln 3 (\Omega)$ . The transformed impedance  $Z_b$  is also plotted in the same Smith chart. It is observed that the impedance loop now is moved to the center of the Smith chart, which means a good impedance match. Note that  $Z_b$  is essentially equal to the odd-mode impedance  $Z_o$  if neglecting the radiation from the “transmission line” (note that the separation between the feed probe and the shorting pin should be kept as small as possible to reduce the spurious radiation from the “transmission line”). Since the odd-mode impedance is dominant over the SBA band,  $Z_b$  should be very close to the unbalance-fed input impedance  $Z_{in}$ , which is also plotted (dotted line) in the Smith chart. Indeed  $Z_b$  and  $Z_{in}$  show good agreement.

To better understand the matching mechanism, a diagram illustration for the matching procedure is drawn in the Smith chart. For a large impedance (e.g., an impedance point A at the loop center of impedance  $Z_s$ ), when it is normalized to  $Z_c$ , point A moves to point B. Note that normalized impedance is decreased since  $Z_c (\cong 130 \Omega)$  is much larger than  $50 \Omega$ . After clockwise rotating by an angle of  $2\beta H_s \cong 4\pi/3$ , point B reaches to point C. This is the normalized (to  $Z_c$ ) impedance after applying the transmission-line formula (3). If transformed back to the  $50\text{-}\Omega$  system, point C shifts to the center of the Smith chart, reaching to the matching point. This diagram illustration qualitatively explains why we optimize the length of the feed probe and the shorting pin to  $0.32\lambda_0$ , which leads to an overall antenna height of higher than  $0.5\lambda_0$ . Since a slot antenna with a slot length of much less than half a wavelength always has inductive impedance, point A should be always located at the upper part of the Smith chart. In order to move from point A to point C through point B, it is necessary to rotate by an angle larger than  $\pi$ . This means that the height of the slot must be higher than a quarter-wavelength unless using a curved feed probe (to increase its length physically) or a dielectric loaded “transmission line” (to increase its length electrically).

## V. PARAMETRIC STUDY

After understanding the operating principle of the slot-excited SBA, the parametric study is straightforward. Most SBA-related publications have focused on the study of the radiation characteristics. Despite the difference in the excitation structure, the proposed SBA shares a similar mechanism for the backfire radiation with all other types of SBA. As a result, we only need to investigate the impedance performance. For the slot-excited SBA, the input impedance is affected in a larger degree by the slot and the unbalanced probe feed (including the probe and the shorting pin) than by other components such as the reflectors and the rim. Based on this consideration, we concentrate our investigation on the effects of the:

- height of the slot ( $H_s$ );
- total length of the slot ( $l_s$ );
- width of the slot ( $w_s$ );
- width of the central part of the slot ( $w_c$ );
- length of the central part of the slot ( $l_c$ );

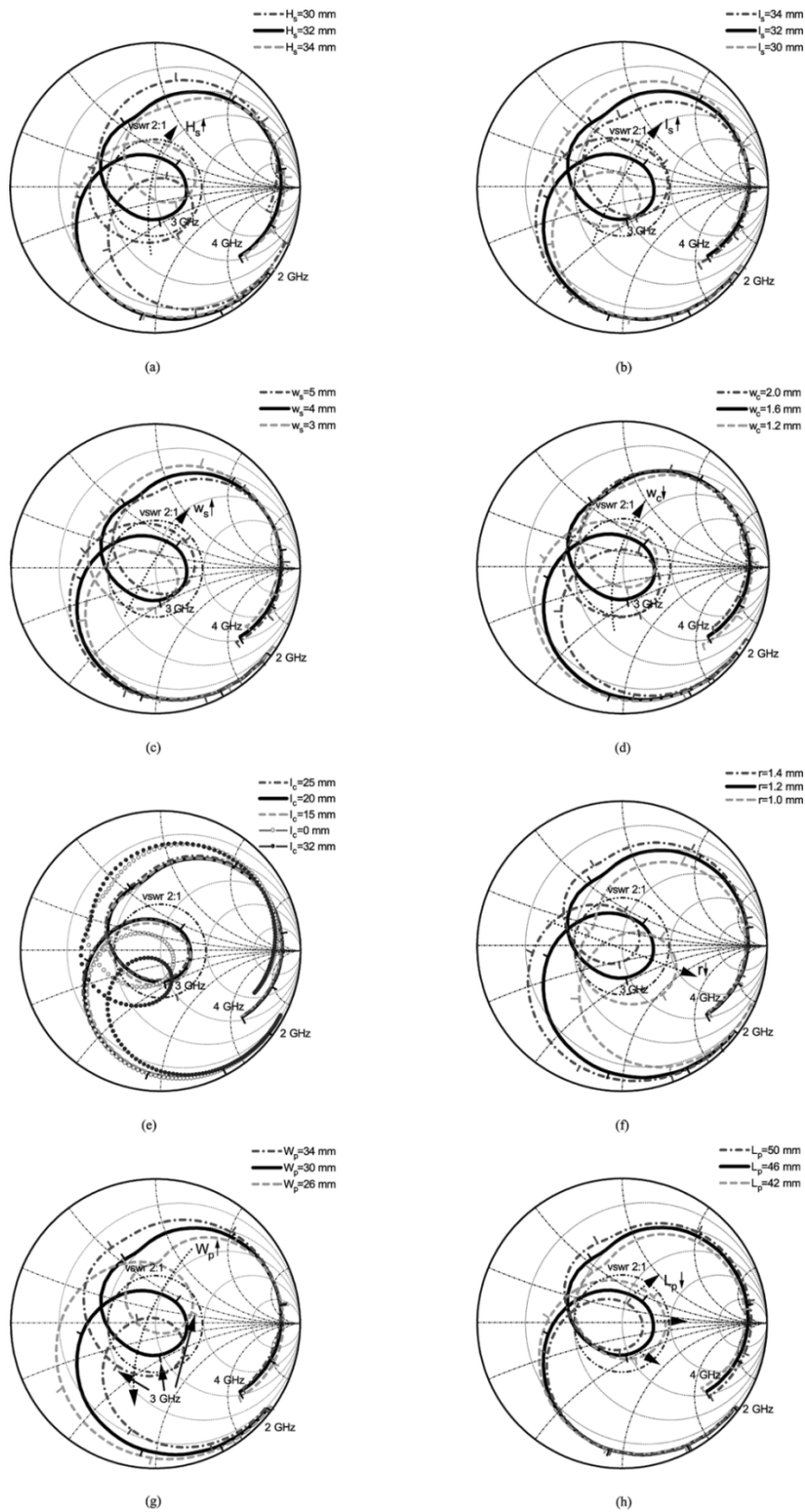


Fig. 11. Effects of the geometric parameters of the slot-excited SBA on its impedance performance. Effect of (a) the height of the slot ( $H_s$ ), (b) the total length of the slot ( $l_s$ ), (c) the width of the slot ( $w_s$ ), (d) the width of the central part of the slot ( $w_c$ ), (e) the length of the central part of the slot ( $l_c$ ), (f) the thickness of the feed probe and shorting pin ( $r$ ), (g) the width of the slotted patch ( $W_p$ ), and (h) the length of the slotted patch ( $L_p$ ).

- f) thickness of the feed probe and shorting pin ( $r$ );
- g) width of the slotted patch ( $W_p$ );
- h) length of the slotted patch ( $L_p$ ).

We did not include the effects of the distance ( $d$ ) between the feed probe and the shorting pin since the low-cross-polarization pattern requires the distance be as short as possible. Depending

on the mechanical process in practical fabrication, at least a 1–2 mm gap (1.6 mm in our fabrication) may be required between the feed probe and the shorting pin. A slight variation of all above parameters has little effect on the radiation performance. In the parametric study, each time only one parameter varies near its optimized value while all other parameters are fixed at their optimized values.

The simulation results for the input impedance are plotted on a Smith chart for each geometric parameter, as shown in Fig. 11. From Fig. 11(a), we can see that the loop of the impedance loci moves up as  $H_s$  increases. This is due to the extension of the “transmission line,” which makes the impedance loop overrotate. Fig. 11(b) shows a slight moveup tendency as  $l_s$  increases. This can be understood by checking up Fig. 10. An increase in  $l_s$  causes point A in Fig. 10 to move down due to the decreased inductive component of the input impedance. Following the impedance matching procedure indicated in Fig. 10, it is easy to find that the impedance loop will overrotate. It is also noted that the size of the loop increases with  $l_s$ . This means we cannot make the slot too long. From our experience,  $l_s$  should be less than  $0.35\lambda_0$ .

A similar explanation applies to Fig. 11(c) and (d) where the impedance loop also squints up as  $w_s$  widens or  $w_c$  becomes narrower. Fig. 11(e) shows that the impedance loop is not sensitive to the length of the central part of the slot ( $l_c$ ). This is reasonable because a variation of  $l_c$  will not change the perimeter (always  $= 2l_s + 4w_s - 2w_c$ ) of the slot, thus not causing a significant change in the trace along which the current flows. Note that a certain length of  $l_c$  is necessary for maintaining the form of the H-shaped slot. Otherwise the H-shaped slot deforms to a rectangular slot and its perimeter becomes  $2l_s + 2w_s$  or  $2l_s + 2w_c$ , which results in a considerable difference in the current flow. As a result, the impedance performance will be changed. This can be observed from Fig. 11(e), where the cases of  $l_c = 0$  and 32 mm correspond to a rectangular slot with a slot width of 4 and 2.4 mm, respectively. It can be seen that the impedance loop obviously shifts away from the center of the Smith chart. Both simulation and experiment have demonstrated that it is difficult to achieve a wide-band performance with a rectangular slot.

The effect of the thickness of the feed probe (and shorting pin) is demonstrated in Fig. 11(f). We can see that as the feed probe becomes thinner, the input resistance tends to increase. The reason is explained as follows. As  $r$  decreases, the characteristic impedance  $Z_c$  of the “transmission line” increases and the normalized impedance decreases. As a result, both points B and C (see Fig. 10) move closer to the center of the Smith chart. Note that moving point B toward the Smith-chart center means a decreased impedance while the same movement tendency for point C means an increased normalized resistance. Eventually the input resistance increases since it equals the increased characteristic impedance  $Z_c$  multiplied by the increased normalized resistance.

Fig. 11(g) and (h) reflects the effect of the size of the patch that supports the slot. We observe that as the patch width ( $W_p$ ) increases, the impedance loop moves down and the frequency shifts down. This may be due to the increase in capacitance as the patch becomes larger. The effect of the patch length ( $L_p$ )

is not significant but the size of the impedance loop shrinks as the length increases, probably due to the enhanced coupling between the patch and the subreflector. Therefore an increase in the patch length may be helpful in lowering the VSWR level.

## VI. CONCLUSION

A novel excitation configuration for the short backfire antenna is developed. The excitation structure consists of an H-shaped slot and a simple probe feed. The slot-excited SBA achieves an impedance bandwidth of 20% for  $VSWR < 2$ . Over this bandwidth, the antenna has a gain ranging from 13.5 to 15.5 dBi, a backside level of less than  $-25$  dB, and sidelobes lower than  $-20$  dB. Simulation and experimental results show good agreement. The operating principle is investigated based on the analysis of mode decomposition. The mechanism for impedance matching is analyzed to better understand the features of the antenna. The parametric study demonstrates the effects of different geometric parameters on the impedance performance, which may be useful in practical engineering design.

## REFERENCES

- [1] H. W. Ehrenspeck, “The backfire antenna, a new type of directional line source,” *Proc. IRE*, vol. 48, no. 1, pp. 109–110, Jan. 1960.
- [2] —, “The short-backfire antenna,” *Proc. IEEE*, vol. 53, pp. 1138–1140, Aug. 1965.
- [3] K. M. Chen, D. P. Nyquist, and J. L. Lin, “Radiation fields of the short-backfire antenna,” *IEEE Trans. Antenna Propag.*, vol. 16, pp. 596–597, Sep. 1968.
- [4] Y. Yamada, T. Takan, and N. Ishida, “Compact antenna equipment for maritime satellite communication systems,” *Trans. IEICE*, vol. 62-B, pp. 844–846, 1979.
- [5] S. Yang, S. H. Tan, and J. S. Fu, “Short backfire antennas for wireless LAN applications at millimeter-waves,” in *IEEE AP-S Int. Symp.*, vol. 3, Jul. 2000, pp. 1260–1263.
- [6] G. P. Heckert, “Investigation of L-band shipboard antennas for maritime satellite applications,” *Automated Marine Int. Rep. NASW-2165*, Feb. 1972.
- [7] S. Ohmori, S. Miura, K. Kameyama, and H. Yoshimura, “An improvement in electrical characteristics of a short backfire antenna,” *IEEE Trans. Antennas Propag.*, vol. AP-31, pp. 644–646, Jul. 1983.
- [8] *Mobile Antenna Systems Handbook*, 2nd ed., K. Fujimoto and J. R. James, Eds., Artech House, Norwood, MA, 2000, pp. 542–545.
- [9] A. A. Kishk and L. Shafai, “Gain optimization of short-backfire antenna with different excitation types,” in *IEEE AP-S Int. Symp.*, vol. 24, Jun. 1986, pp. 923–926.
- [10] M. S. Leong, P. S. Kooi, P. S. Chandra, and T. S. Yeo, “Theoretical and experimental investigations of two-dimensional waveguide-excited short backfire antenna structure,” *Proc. Inst. Elect. Eng. H*, vol. 136, no. 3, Jun. 1989.
- [11] Z. N. Chen and M. Y. W. Chia, “A center-slot-fed suspended plate antenna,” *IEEE Trans. Antennas Propag.*, vol. 51, pp. 1407–1410, Jun. 2003.
- [12] S. Gao, L. W. Li, M. S. Leong, and T. S. Yeo, “A broad-band dual-polarized microstrip patch antenna with aperture coupling,” *IEEE Trans. Antennas Propag.*, vol. 51, pp. 898–900, Apr. 2003.
- [13] G. P. Otto, C. Lu, and W. C. Chew, “Circular short backfire antenna modeling,” *IEEE Trans. Antennas Propag.*, vol. 40, pp. 1434–1438, Nov. 1992.
- [14] M. Rayner, A. D. Olver, and A. D. Monk, “FD-TD design of short backfire antennas,” *Proc. Inst. Elect. Eng. Microwave Antennas Propag.*, vol. 144, no. 1, pp. 1–6, Feb. 1997.
- [15] R. E. Collin, *Antennas and Radiowave Propagation*. New York: McGraw-Hill, Jan. 1985, pp. 93–97.
- [16] U. S. Inan and A. S. Inan, *Engineering Electromagnetics*. Reading, MA: Addison-Wesley, 1999, p. 85.



**RongLin Li** (M'02–SM'03) received the B.S. degree in electrical engineering from Xi'an Jiaotong University, China, in 1983 and the M.S. and Ph.D. degrees in electrical engineering from Chongqing University, China, in 1990 and 1994, respectively.

From 1983 to 1987, he was an Electrical Engineer with the Yunnan Electric Power Research Institute. From 1994 to 1996, he was a Postdoctoral Research Fellow with Zhejiang University, China. In 1997, he was with Hosei University, Japan, as a Hosei International Fund Research Fellow. Since 1998, he has been a Professor with Zhejiang University. In 1999, he was a Research Associate with the University of Utah. In 2000, he was a Research Fellow with Queen's University of Belfast, U.K. In 2001, he joined the ATHENA group as a Research Scientist with the Georgia Institute of Technology, Atlanta. His latest research interests include computational electromagnetics, modeling of antennas and microwave devices, and RF packaging design.



**Dane Thompson** (S'03) received the B.S. and M.S. degrees in electrical engineering from Santa Clara University, Santa Clara, CA, in 2001 and 2002, respectively. He is currently pursuing the Ph.D. degree in electrical and computer engineering at the Georgia Institute of Technology, Atlanta.

He is currently a Graduate Research Assistant. His research involves RF front-ends on multilayer organic substrates including antennas, filters, passives, MEMS, and packaging structures.



**Manos M. Tentzeris** (S'89–M'98–SM'03) received the diploma degree in electrical and computer engineering from the National Technical University of Athens, Greece, and the M.S. and Ph.D. degrees in electrical engineering and computer science from the University of Michigan, Ann Arbor.

He is currently an Associate Professor with the School of Electrical and Computer Engineering, Georgia Institute of Technology (Georgia Tech), Atlanta. He has published more than 140 papers in refereed journals and conference proceedings

and six book chapters. He has helped develop academic programs in highly integrated packaging for RF and wireless applications, microwave MEMS, SOP-integrated antennas and adaptive numerical electromagnetics (FDTD, multiresolution algorithms). He is the Georgia Tech NSF-Packaging Research Center Associate Director for RF Research and the RF Alliance Leader. He is also the Leader of the Novel Integration Techniques Subthrust of the Broadband Hardware Access Thrust of the Georgia Electronic Design Center (GEDC) of the State of Georgia. He was a Visiting Professor with the Technical University of Munich, Germany, for summer 2002.

Dr. Tentzeris is a member of URSI Commission D, an Associate Member of EuMA, and a member of the Technical Chamber of Greece. He received the 2004 IBA International Educator of the Year Award, the 2003 IEEE CPMT Outstanding Young Engineer Award, the 2002 International Conference on Microwave and Millimeter-Wave Technology Best Paper Award (Beijing, China), the 2002 Georgia Tech-ECE Outstanding Junior Faculty Award, the 2001 ACES Conference Best Paper Award, the 2000 NSF CAREER Award, and the 1997 Best Paper Award, International Hybrid Microelectronics and Packaging Society. He was also the 1999 Technical Program Cochair of the 54th ARFTG Conference, Atlanta, GA, and he is Vice-Chair of the RF Technical Committee (TC16) of the IEEE CPMT Society.



**Joy Laskar** (S'84–M'85–SM'02) received the B.S. degree in computer engineering (math/physics minors, highest honors) from Clemson University, Clemson, SC, in 1985 and the M.S. and Ph.D. degrees in electrical engineering from the University of Illinois, Urbana-Champaign, in 1989 and 1991, respectively.

Prior to joining the Georgia Institute of Technology (Georgia Tech), Atlanta, in 1995, he held faculty positions at the University of Illinois and the University of Hawaii. At Georgia Tech, he holds the

Joseph M. Pettit Professorship of Electronics, is currently the Chair for the Electronic Design and Applications Technical Interest Group, the Director of Georgia's Electronic Design Center and the System Research Leader for the NSF Packaging Research Center. His research has focused on high frequency IC design and their integration. He also heads a research group with a focus on integration of high-frequency electronics with optoelectronics and integration of mixed technologies for next generation wireless and optoelectronic systems. He has authored or coauthored more than 200 papers, several book chapters (including three textbooks in development), numerous invited talks, and has 10 patents pending. In 1998, he cofounded an advanced WLAN IC Company: RF Solutions, which is now part of Anadgics (Nasdaq: Anad). In 2001, he cofounded a next generation interconnect company: Quellan, which is developing collaborative signal processing solutions for enterprise applications.

Dr. Laskar is a 1995 recipient of the Army Research Office's Young Investigator Award, a 1996 recipient of the National Science Foundation's CAREER Award, the 1997 NSF Packaging Research Center Faculty of the Year, the 1998 NSF Packaging Research Center Educator of the Year, the 1999 corecipient of the IEEE Rappaport Award (Best IEEE Electron Devices Society Journal Paper), the faculty advisor for the 2000 IEEE MTT IMS Best Student Paper award, 2001 Georgia Tech Faculty Graduate Student Mentor of the year, recipient of a 2002 IBM Faculty Award, the 2003 Clemson University College of Engineering Outstanding Young Alumni Award and the 2003 recipient of the Outstanding Young Engineer of the Microwave Theory and Techniques Society. He has been named the Joseph M. Pettit Professor of Electronics in the School of Electrical and Computer Engineering at Georgia Tech. For the 2004–2006 term, he has been appointed an IEEE Distinguished Microwave Lecturer for his seminar entitled "Recent Advances in High Performance Communication Modules and Circuits."



**John Papapolymerou** (S'90–M'99–SM'04) received the B.S.E.E. degree from the National Technical University of Athens, Athens, Greece, in 1993, and the M.S.E.E. and Ph.D. degrees from the University of Michigan, Ann Arbor, in 1994 and 1999, respectively.

From 1999 to 2001, he was a faculty member at the Department of Electrical and Computer Engineering of the University of Arizona, Tucson, and during summer 2000 and 2003 he was a Visiting Professor at The University of Limoges, France. In August

2001, he joined the School of Electrical and Computer Engineering, Georgia Institute of Technology, Atlanta, where he is currently an Assistant Professor. He has authored or co-authored over 80 publications in peer reviewed journals and conferences. His research interests include the implementation of micro-machining techniques and MEMS devices in microwave, millimeter-wave and THz circuits and the development of both passive and active planar circuits on Si and GaAs for high-frequency applications.

Dr. Papapolymerou received the 1997 Outstanding Graduate Student Instructional Assistant Award presented by the American Society for Engineering Education (ASEE), The University of Michigan Chapter, the 2002 NSF CAREER award, the best paper award at the 3rd IEEE International Conference on Microwave and Millimeter-Wave Technology (ICMMT2002), Beijing, China, and the 2004 ARO Young Investigator Award. He currently serves as the secretary for Commission D of the U.S. National Committee of the URSI.